MAGNETIC RESONANCE STUDY OF RADIATION-INDUCED LITHIUM ATOMS IN CRYSTALLINE SiO_2

By

MARK SHANNON GULLEY

Bachelor of Arts

Hendrix College

Conway, Arkansas

1985

Submitted to the Faculty of the
Graduate College of the
Oklahoma State University
in partial fulfillment of
the requirements for
the Degree of
MASTER OF SCIENCE
December, 1987

MAGNETIC RESONANCE STUDY OF RADIATION-INDUCED LITHIUM ATOMS IN CRYSTALLINE SiO_2

Thesis Approved:

Larry E. Halliburton
Thesis Advisor

Joel J. Martin

Norman N. Durham
Dean of the Graduate College

ACKNOWLEDGEMENTS

I would like to gratefully acknowledge my advisor, Dr. L. E. Halliburton, for his kind guidance and patience throughout this project. I would also like to thank Dr. J. J. Martin and Dr. S. W. S. McKeever for serving on my thesis committee. Their support was greatly appreciated.

I would also like to thank Dr. C. Y. Chen for his guidance and advice, Mr. C. A. Hunt for his patience with me in the Crystal Growth Lab, and Dr. Rezza Hantezadeh, Mr. Michael Scripsick, and Mr. George Gangwere for their helpful conversations pertaining to this study. I also wish to express my gratitude to Dr. Paul Westhaus for his encouragement throughout my graduate career.

I wish to especially acknowledge Dr. M. G. Jani, with whom I worked closely on this project. His patience and concern with teaching me how to be a good research scientist are greatly appreciated.

Most importantly, I wish to thank my family for their love, support, and encouragement throughout my education.

Lastly, I would like to acknowledge the Physics Department of Oklahoma State University and the U. S. Air Force for their financial support on this project.

TABLE OF CONTENTS

Chapter		Page
I.	INTRODUCTION	1
	Previous Studies	6
	Present Study	9
II.	EXPERIMENTAL APPARATUS AND PROCEDURE	10
	Sample Preparation and Defect Production	10
	ESR Spectrometer	11
	Procedure	13
	Computer Equipment	13
III.	THEORETICAL ANALYSIS	14
IV.	EXPERIMENTAL RESULTS AND ANALYSIS	21
V.	DISCUSSION	32
A SELECTED BIBLIOGRAPHY		34
APPENDIX A		35
APPENDIX B		44

LIST OF TABLES

Table		Page
I.	Lower Half of the Spin Hamiltonian Matrix.....	20
II.	Spin Hamiltonian Final Parameters.....	31

LIST OF FIGURES

Figure		Page
1.	Schematic Diagram of Alpha-Quartz.....	3
2.	Three Types of Aluminum-Related Defects.....	5
3.	The $[SiO_4/Li]^o$ Center.....	8
4.	Block Diagram of ESR Spectrometer.....	12
5.	ESR Spectrum of the $[AlO_4]^o$ Center and the $[SiO_4/Li]^o$ Center Lines.....	22
6.	Enlargement of $[SiO_4/Li]^o$ Center Line Spectrum.....	23
7.	ESR Spectrum of High and Low Field Regions of the $[SiO_4/Li]^o$ Center.....	25
8.	Angular Dependence Study of Lines in High and Low Field Regions.....	26
9.	Energy Level Diagram of S=1/2, I_1=3/2, and I_2=1/2 System.....	28

CHAPTER I

INTRODUCTION

Quartz is one of the many crystals found in nature that exhibit the phenomenon known as piezoelectricity. In a piezoelectric material, electrical polarization is produced by mechanical stress. This is also a reversible process, wherein an applied electric field will produce a strain. A large number of piezoelectric materials have been characterized over the last half-century, but as of yet only a few are widely used as precision frequency control devices. Alpha-quartz is used for precision bulk piezoelectric resonators and surface-acoustic-wave (SAW) devices [1].

Alpha-quartz, a specific crystalline form of silica (SiO_2), is the only variant of SiO_2 having application in frequency control. Alpha-quartz is also known as low quartz; this refers to the fact that it exists at temperatures less than 573°C. Alpha-quartz has a trigonal crystal symmetry and belongs to point group 32. Both right- and left-handed alpha-quartz exist, corresponding to space groups $P3_221$ and $P3_121$, respectively. The general alpha-quartz structure consists of SiO_4 tetrahedra that share each of their corners with another tetrahedron [2]. Alpha-

quartz has an axis of threefold symmetry, which is commonly called the c axis or optic axis. Also, three equivalent twofold axes lie 120 degrees apart in a plane perpendicular to the optic axis. This is the natural coordinate system of alpha-quartz. A Cartesian coordinate system is also chosen for quartz such that the Z and X axes are parallel to the optic axis and one of the twofold axes, respectively. The Y axis is then chosen to form a right-handed coordinate system [1]. Figure 1 is a diagram of the crystal structure of alpha-quartz.

Quartz is found in nature as large crystals. Arkansas and Brazil are two areas well-known for having abundant quartz crystals. However, quartz has also been grown commercially since World War II. The quartz used in this study is synthetic quartz. The process used for growing quartz is called hydrothermal growth. The lower zone of an autoclave contains natural quartz fragments at high temperature to be used as a nutrient and the upper zone of the autoclave contains seed plates at a slightly lower temperature. Either a sodium hydroxide or a sodium carbonate solution is used to dissolve the nutrient and transport material up to the upper zone. Temperatures are about $350^{o}C$, the autoclave pressure is roughly 1×10^{8} Pa, and growing periods range from one to over three months [2].

There are a variety of impurities in quartz, but the two that are important in this study are the substitutional aluminum and the interstitial lithium. An aluminum 3+ ion

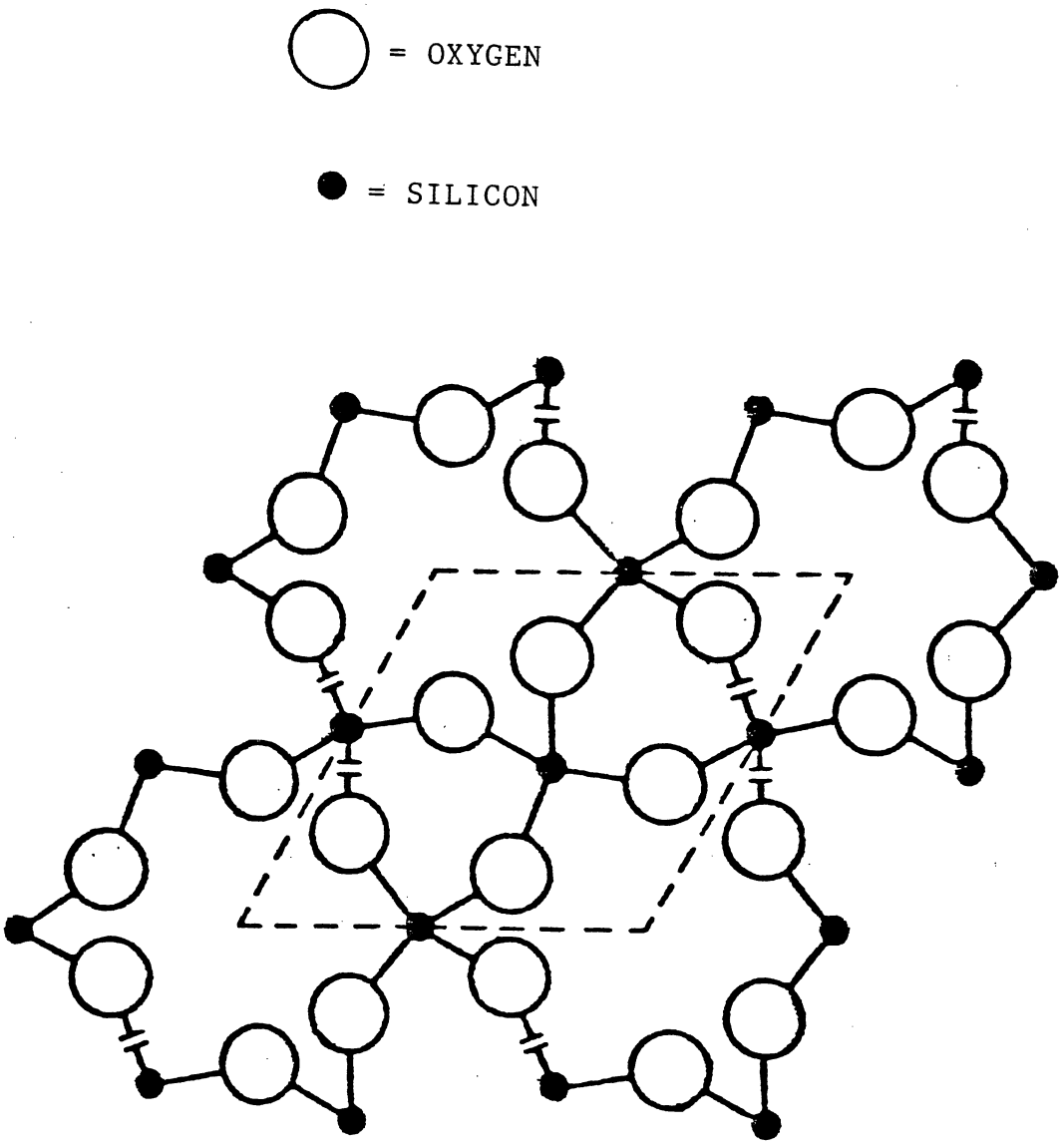

Figure 1. Schematic Diagram of Alpha-Quartz

can easily substitute for a silicon 4+ ion. Since the aluminum has one less positive charge than the silicon, it requires some type of charge compensator. Four of the aluminum charge compensators known to exist in quartz are H^+, Li^+, and Na^+ ions at interstitial sites and holes trapped at oxygen ions. Typically, one of these charge compensators is located next to each substitutional aluminum ion, thus giving rise to $[AlO_4/H^+]^o$, $[AlO_4/Li^+]^o$, $[AlO_4/Na^+]^o$, or $[AlO_4]^o$ centers. Here I am using the notation proposed by Weil [3]. A schematic representation of these defect centers is shown in figure 2.

These defect centers have been observed by a variety of experimental techniques. In the case of the $[AlO_4/H^+]^o$ center, which consists of an interstitial proton bound to an oxygen ion to form an OH^- molecule, stretching vibrations of the OH^- molecule cause infrared absorptions at wavenumbers 3367 and 3306 cm^{-1}.

An $[AlO_4/Li^+]^o$ or an $[AlO_4/Na^+]^o$ center consists of an aluminum ion with an adjacent interstitial lithium or sodium ion in the optic axis channel. This type of defect can give rise to one or more characteristic acoustic loss peaks because of the stress-induced motion of the lithium or sodium ion from one equilibrium position to another about the aluminum ion. King [4] and Fraser [5] have related an acoustic loss peak at 50 K to the $[AlO_4/Na^+]^o$ center. Stevels and Volger [6] and Nowick et al. [7] have described the dielectric loss of this defect center. The $[AlO_4/Li^+]^o$ center

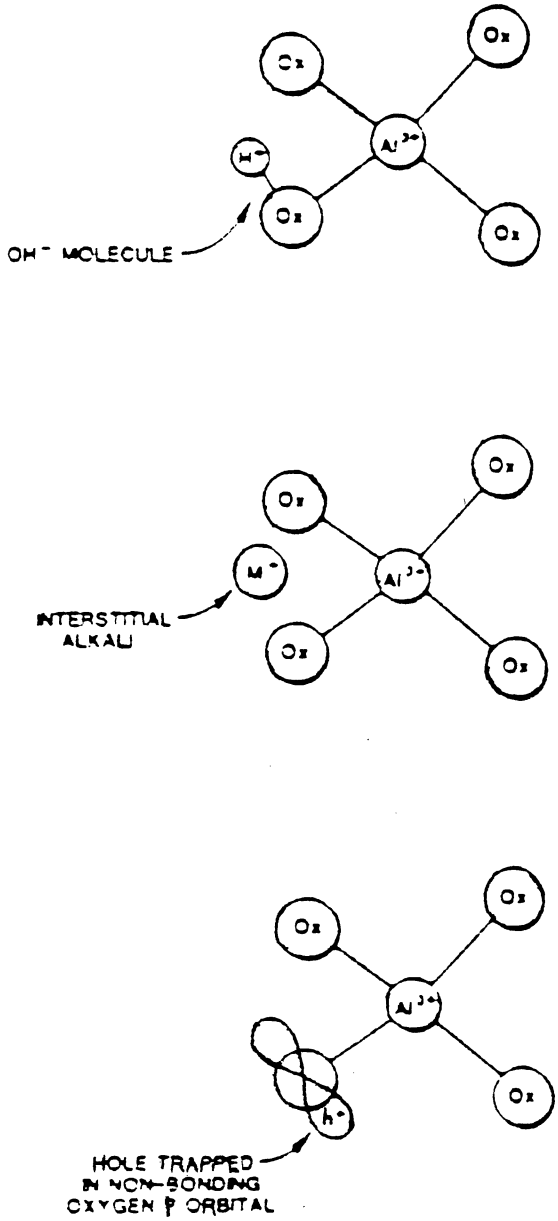

Figure 2. Three Types of Aluminum-Related Defects

does not seem to have dielectric and acoustic loss peaks. Toulouse et al. [8] suggested that these peaks are not observed because the lithium ion resides on the twofold symmetry axis of the AlO_4 tetrahedron to which it is bound.

A hole trapped in a non-bonding p orbital of an oxygen ion located adjacent to the aluminum forms the $[AlO_4]^o$ center. This center is easily detected by electron spin resonance because the oxygen has an unpaired electron. In this study, the $[AlO_4]^o$ center was used to align the magnetic field along the crystal's c axis [2].

There have been a number of previous studies leading up to the present investigation. The following paragraphs outline the most significant papers that relate to the present study.

Previous Studies

Initial Observations

The $[SiO_4/Li]^o$ center was observed and studied by Jani et al. [9] using electron spin resonance. This center was produced by an initial irradiation at a temperature between 150 K and 300 K which released the lithium ion from its associated Al^{3+} ion and then a second irradiation at 77 K to trap an electron at the new location of the lithium ion (which is by a silicon ion). The g values for the defect were electronlike and there was a weak hyperfine splitting

due to a single ^{7}Li nucleus and a strong hyperfine splitting due to a single ^{29}Si nucleus. These results prompted them to suggest that the defect was an electron stabilized by an interstitial lithium ion with the unpaired spin density localized primarily on one of the adjacent four-coordinated silicon ions. These investigators conducted an angular dependence study of the central four-line spectrum and determined the parameters for the g tensor and for the A tensor corresponding to the lithium hyperfine interaction. Figure 3 shows a schematic diagram of this defect center.

Correlation of ESR and TL

A study of the $[SiO_4/Li]^{o}$ center was performed by Halperin et al. [10] in which the results from thermoluminescence and electron spin resonance experiments were compared. A large thermoluminescence peak near 190 K was observed to be formed by the same double-irradiation procedure that was necessary to produce the ESR signal attributed to the $[SiO_4/Li]^{o}$ center. They concluded that the peak at 190 K was caused by electrons being released by the $[SiO_4/Li]^{o}$ center and recombining with holes at unidentified defects.

Theoretical Model

A theoretical investigation of the $[SiO_4/Li]^{o}$ center previously reported by Jani et al. [9] was conducted by Wilson et al. [11]. A 19-atom cluster was used in a quantum chemistry calculation designed to model the center. Slater-

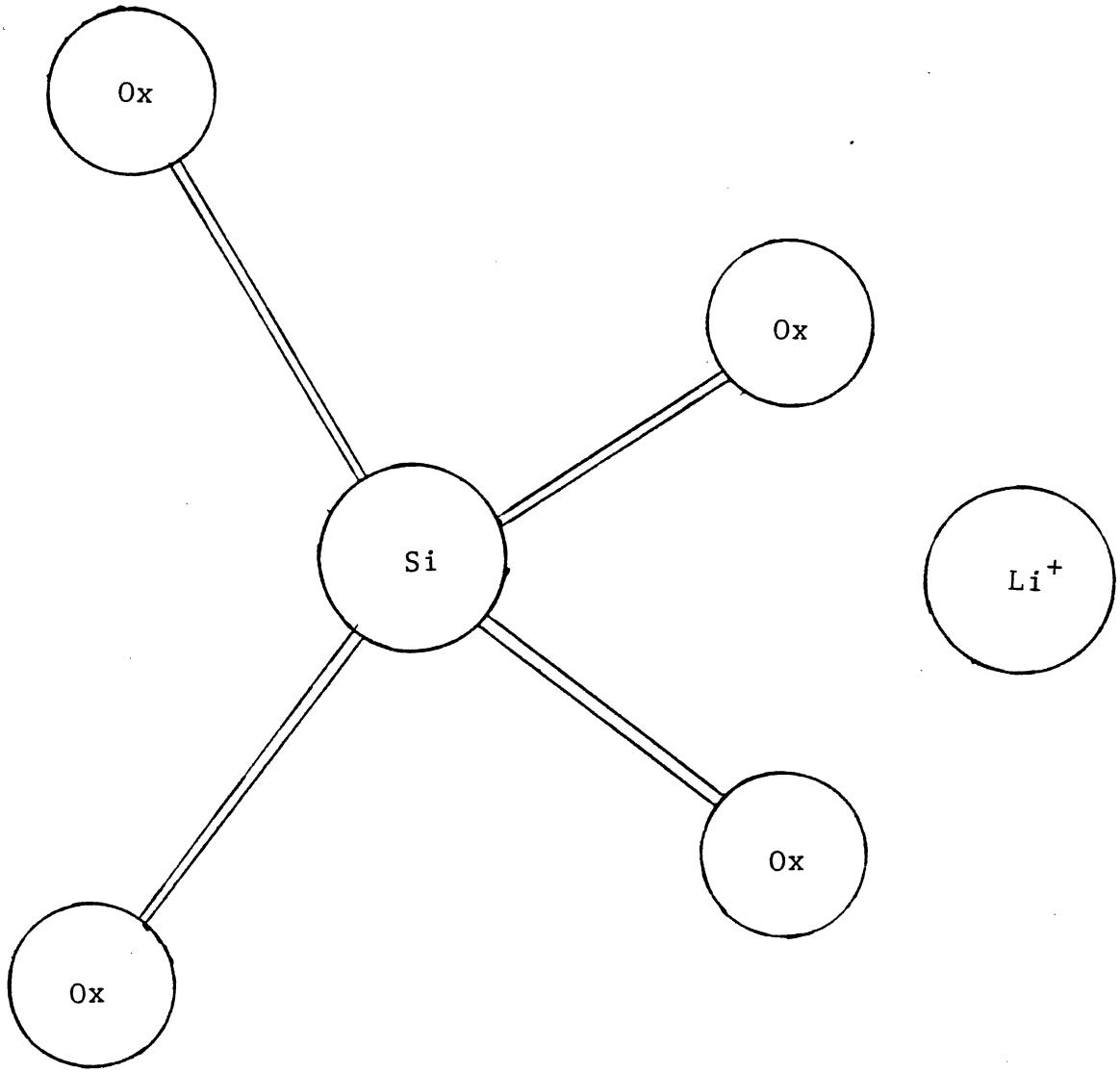

Figure 3. The $[SiO_4/Li]^o$ Center

type orbitals and a three-Gaussian basis set (STO-3G) were used to determine the equilibrium positions of the lithium, silicon, and oxygen atoms. Then, a STO-6G basis set was used to determine the charge and spin densities. The results indicated that the spin density of the unpaired electron was concentrated on the silicon atom, whereas the charge density was concentrated on the lithium atom.

Observation of a Na Version

A thermoluminescence peak at 202 K was observed by Halperin and Katz [12] in quartz that had been electro-diffused with sodium. This peak was observed after the same double-irradiation procedure used to produced the 190-K thermoluminescence peak in lithium-rich quartz. They suggested that this peak was related to the $[SiO_4/Na]^o$ center in analogy to the relation between the 190 K peak and the $[SiO_4/Li]^o$ center. Further study of the $[SiO_4/Na]^o$ center with ESR is needed to verify this result.

Present Study

In this study, we have continued the electron spin resonance study of the $[SiO_4/Li]^o$ center. Angular measurements were made of the ^{29}Si hyperfine interaction.

CHAPTER II

EXPERIMENTAL APPARATUS AND PROCEDURE

Sample Preparation and Defect Production

The synthetic quartz crystals used in this study were obtained from ThermoDynamics, Shawnee Mission, KS. For the ESR studies, the samples were cut to dimensions of 8mm x 2.5mm x 3mm in the X, Y, and Z directions, respectively, by using a diamond saw in the Crystal Growth Laboratory at Oklahoma State University. All samples were taken from the x-growth region of the stone. This region was identified by irradiating a slice of the bar from which the samples were to be cut and then examining the visible coloration.

Samples were irradiated with 1.5-MeV electrons at a current of 2 microamperes from a Van de Graaff electron accelerator. The irradiation procedure consisted of two irradiations: one at 200 K and the other at 77 K. The sample was placed in a styrofoam cup which was then filled with frozen carbon dioxide (dry ice) and irradiated for 5 minutes. The dry ice was then quickly replaced with liquid nitrogen and another 5-minute irradiation was performed. The rapid change from dry ice to liquid nitrogen is neces-

sary in order to keep the sample from warming up and allowing the lithium ions to diffuse to more stable trapping sites. For all irradiations, the sample was placed approximately 50 cm from the aluminum exit window of the accelerator tube.

ESR Spectrometer

All electron spin resonance measurements were made on an IBM Instruments (Bruker) ER200D X-band homodyne spectrometer with the sample at liquid nitrogen temperature. The magnet of this spectrometer is water-cooled and capable of producing magnetic fields of over 10,000 gauss. On a platform above the magnet is a Bruker ER044 MRDH microwave bridge, from which a waveguide leads down between the magnet pole pieces. Attached to the waveguide is a TE 102 rectangular microwave cavity, which is the cavity used for all the measurements made in this study. The TE 102 is a commercial cavity equipped with Helmholtz coils for 100-kHz modulation. Also part of the ER200D system are the magnet power supply, the cooling water circulation unit, and the main console, which contains a timebase unit, a signal channel, magnetic field controller, and a chart recorder. A block diagram of the ESR spectrometer is shown in figure 4.

For final measurements, magnetic fields were measured with a Varian E-500 Gaussmeter. The gaussmeter consisted of a marginal oscillator and a proton probe. The probe was

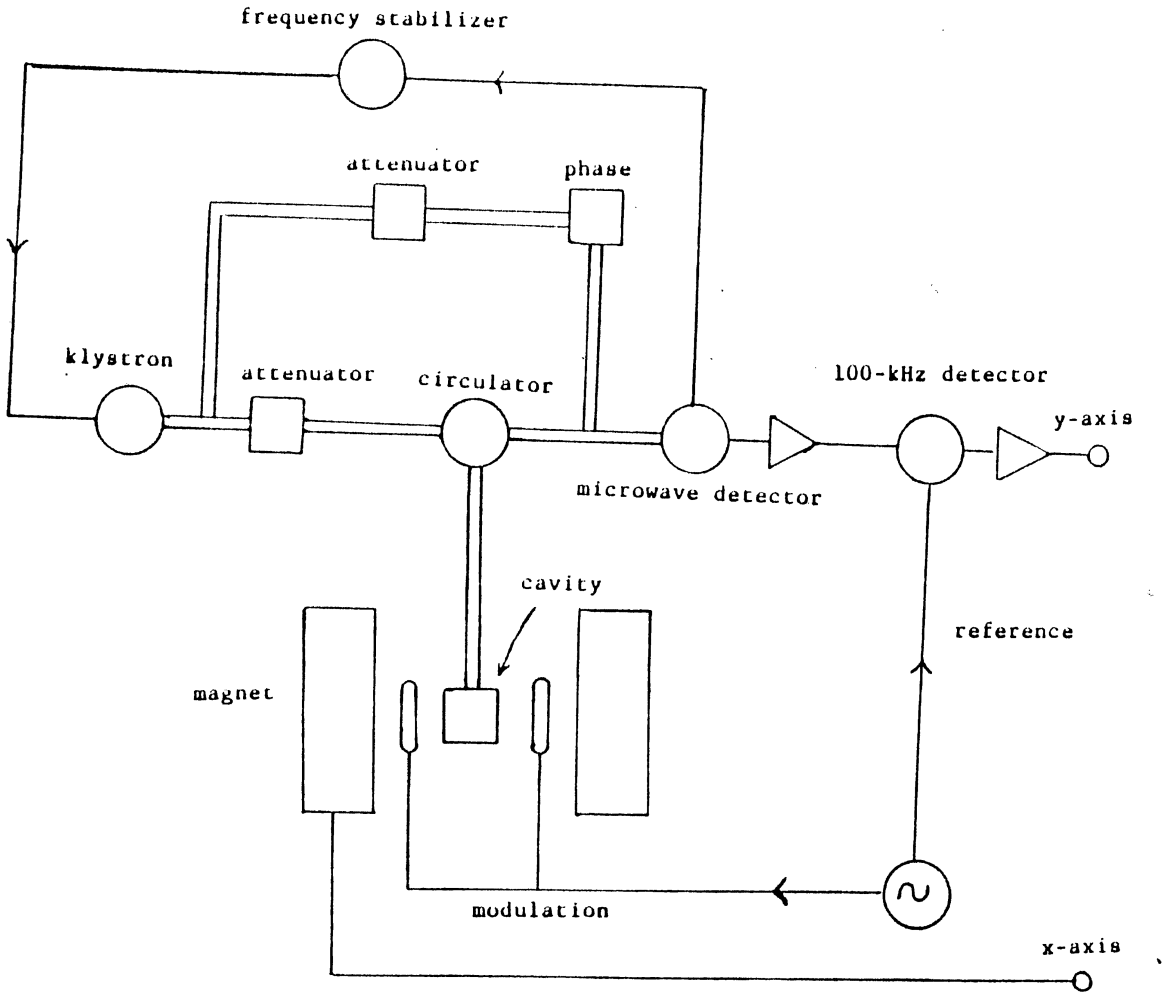

Figure 4. Block Diagram of ESR Spectrometer

attached rigidly between the faces of the magnet. Measurements of the main line of a standard $MgO:Cr^{3+}$ sample were made at the various angles used in the angular dependence study to correct the measured field values since the probe was not located at the same spot as the sample. The known g-value for $MgO:Cr^{3+}$ is 1.9799. To measure the microwave frequency, a Hewlett Packard 5340A frequency counter was connected directly to the microwave bridge.

Procedure

After irradiation, the sample was placed in a finger Dewar filled with liquid nitrogen. The Dewar was placed in the cavity and the aluminum-hole center was found. The aluminum-hole center was used to align the c axis of the sample parallel to the magnetic field. The ^{29}Si hyperfine spectrum was then found and recorded on chart paper. The magnet was then rotated to a new angle to take another spectrum. In order to cover a full 70^{o} of rotation, the coaxial cables attached to the cavity were unhooked and re-attached to the cavity by means of single wires so that the cables would hang down and out of the way of the rotating magnet.

Computer Equipment

The computer used to analyze data was a Hewlett Packard 9000 (Series 300) programmed in compiled BASIC 4.0.

CHAPTER III

THEORETICAL ANALYSIS

We assume that the system under study can be described by the following spin Hamiltonian:

$$\mathcal{H} = \beta \vec{H} \cdot \overleftrightarrow{g} \cdot \vec{S} + \vec{I}_1 \cdot \overleftrightarrow{A} \cdot \vec{S} + \vec{I}_2 \cdot \overleftrightarrow{A} \cdot \vec{S} - (g_N \beta_N)_1 \vec{H} \cdot \vec{I}_1 - (g_N \beta_N)_2 \vec{H} \cdot \vec{I}_2$$

This is a general spin Hamiltonian for a system with one electron of spin S and two nuclei of spins I_1 and I_2. For the system in this study, S=1/2, I_1=3/2, and I_2=1/2. The first term in the Hamiltonian represents the electron Zeeman interaction, the second and third terms represent the nuclear hyperfine interactions, and the last two terms represent the nuclear Zeeman interactions.

The following coordinate systems are used to convert the spin Hamiltonian into a form suitable for numerical analysis by a computer program.

x,y,z: Coordinate system of the magnetic field (chosen so that H is parallel to the z axis.)

x_c, y_c, z_c: Crystal coordinate system

x_g, y_g, z_g: Principal axes of the g tensor

x_1, y_1, z_1: Principal axes of the ^{7}Li hyperfine tensor, A_1

x_2, y_2, z_2: Principal axes of the ^{29}Si hyperfine tensor, A_2

The spin Hamiltonian can now be rewritten in terms of the different coordinate systems.

$$\begin{aligned}\mathcal{H} &= \beta(S_{xg}g_{xg}H_{xg} + S_{yg}g_{yg}H_{yg} + S_{zg}g_{zg}H_{zg}) \\ &+ I_{x1}A_{x1}S_{x1} + I_{y1}A_{y1}S_{y1} + I_{z1}A_{z1}S_{z1} \\ &+ I_{x2}A_{x2}S_{x2} + I_{y2}A_{y2}S_{y2} + I_{z2}A_{z2}S_{z2} \\ &- (g_N\beta_N)_1 HI_{z1} - (g_N\beta_N)_2 HI_{z2}\end{aligned}$$

We now wish to transform the coordinate systems into the magnetic field coordinate system by using rotation matrices [TG], [TH], and [TB], such that

$$\begin{bmatrix} x_g \\ y_g \\ z_g \end{bmatrix} = [TG] \begin{bmatrix} x \\ y \\ z \end{bmatrix}$$

$$\begin{bmatrix} x_1 \\ y_1 \\ z_1 \end{bmatrix} = [TH] \begin{bmatrix} x \\ y \\ z \end{bmatrix}$$

$$\begin{bmatrix} x_2 \\ y_2 \\ z_2 \end{bmatrix} = [TB] \begin{bmatrix} x \\ y \\ z \end{bmatrix}$$

We can now write the spin Hamiltonian in terms of the magnetic field coordinate system only:

$$\begin{aligned}\mathcal{H} &= W1S_x + W2S_y + W4I_{1x}S_x + W5I_{1x}S_y + W3S_z \\ &+ W6I_{1x}S_z + W5I_{1y}S_x + W7I_{1y}S_y + W8I_{1y}S_z \\ &+ W6I_{1z}S_x + W8I_{1z}S_y + W9I_{1z}S_z + W10I_{2x}S_x \\ &+ W11I_{2x}S_y + W12I_{2x}S_z + W11I_{2y}S_x + W13I_{2y}S_y \\ &+ W14I_{2y}S_z + W12I_{2y}S_z + W14I_{2y}S_z + W15I_{2z}S_z \\ &-(g_N\beta_N)_1 HI_{1z} - (g_N\beta_N)_2 HI_{2z}\end{aligned}$$

where

$$W1 = \beta H(g_x TG(1,1)TG(1,3)+g_y TG(2,1)TG(2,3)+g_z TG(3,1)TG(3,3))$$

$$W2 = \beta H(g_x TG(1,2)TG(1,3)+g_y TG(2,2)TG(2,3)+g_z TG(3,2)TG(3,3))$$

$$W3 = \beta H(g_x TG(1,3)TG(1,3)+g_y TG(2,3)TG(2,3)+g_z TG(3,3)TG(3,3))$$

$$W4 = A_{1x}TH(1,1)TH(1,1)+A_{1y}TH(2,1)TH(2,1)+A_{1z}TH(3,1)TH(3,1)$$

$$W5 = A_{1x}TH(1,1)TH(1,1)+A_{1y}TH(2,1)TH(2,2)+A_{1z}TH(3,1)TH(3,2)$$

$$W6 = A_{1x}TH(1,1)TH(1,3)+A_{1y}TH(2,1)TH(2,3)+A_{1z}TH(3,1)TH(3,3)$$

$$W7 = A_{1x}TH(1,2)TH(1,2)+A_{1y}TH(2,2)TH(2,2)+A_{1z}TH(3,2)TH(3,2)$$

$$W8 = A_{1x}TH(1,2)TH(1,3)+A_{1y}TH(2,2)TH(2,3)+A_{1z}TH(3,2)TH(3,3)$$

$$W9 = A_{1x}TH(1,3)TH(1,3)+A_{1y}TH(2,3)TH(2,3)+A_{1z}TH(3,3)TH(3,3)$$

$$W10 = A_{2x}TB(1,1)TB(1,1)+A_{2y}TB(2,1)TB(2,1)+A_{2z}TB(3,1)TB(3,1)$$

$$W11 = A_{2x}TB(1,1)TB(1,2)+A_{2y}TB(2,1)TB(2,3)+A_{2z}TB(3,1)TB(3,2)$$

$$W12 = A_{2x}TB(1,1)TB(1,3)+A_{2y}TB(2,1)TB(2,3)+A_{2z}TB(3,1)TB(3,3)$$

$$W13 = A_{2x}TB(1,2)TB(1,2)+A_{2y}TB(2,2)TB(2,2)+A_{2z}TB(3,2)TB(3,2)$$

$$W14 = A_{2x}TB(1,2)TB(1,3)+A_{2y}TB(2,2)TB(2,3)+A_{2z}TB(3,2)TB(3,3)$$

$$W15 = A_{2x}TB(1,3)TB(1,3)+A_{2y}TB(2,3)TB(2,3)+A_{2z}TB(3,3)TB(3,3)$$

We may now rewrite the Hamiltonian in terms of raising and lowering operators

$$S_+ = S_x + iS_y, \quad S_- = S_x - iS_y$$

$$I_+ = I_x + iI_y, \quad I_- = I_x - iI_y$$

The resulting Hamiltonian is

$$\begin{aligned}\mathcal{H} = {} & W3S_z + W9I_{1z}S_z + W15I_{2z}S_z - (g_N\beta_N)_1 HI_{1z} \\ & -(g_N\beta_N)_2 HI_{2z} + Q1^*S_+ + Q1S_- + Q2^*I_{1+}S_+ \\ & + Q3I_{1+}S_- + Q3I_{1-}S_+ + Q4^*I_{1+}S_z + Q4I_{1-}S_z \\ & + Q4^*I_{1z}S_+ + Q4I_{1z}S_- + Q5^*I_{2+}S_+ + Q6I_{2+}S_- \\ & + Q6I_{2-}S_+ + Q5I_{2-}S_- + Q7^*I_{2+}S_z + Q7I_{2-}S_z \\ & + Q7^*I_{2z}S_+ + Q7I_{2z}S_-\end{aligned}$$

where

Q1 = (W1+iW2)/2

Q2 = (W4-W7)/4 + i*W5/2

Q3 = (W4+W7)/4

Q4 = (W6+iW8)/2

Q5 = (W10-W13)/4 + i*W11/2

Q6 = (W10+W13)/4

Q7 = (W12+iW14)/2

The lithium nucleus has $I_1 = 3/2$ and the silicon nucleus has $I_2 = 1/2$. Therefore, the basis set that we choose will be $|M = 1/2, m_1 = 3/2, m_2 = 1/2\rangle$. This basis set consists of sixteen eigenvectors, which means the Hamiltonian can be written in a 16 x 16 matrix form. The lower half of the spin Hamiltonian matrix is shown in Table I. The non-zero elements of the lower half of the matrix are:

A(1,1) = W3/2 + 3*W9/4 + W15/4 - 3*$(g_N\beta_N)_1$H/2 - $(g_N\beta_N)_2$H/2

A(2,1) = Q7/2

A(3,1) = $\sqrt{3}$*Q4/2

A(9,1) = Q1 + 3*Q4/2 + Q7/2

A(10,1) = Q5

A(11,1) = $\sqrt{3}$*Q2

A(2,2) = W3/2 + 3*W9/4 - W15/4 - 3*$(g_N\beta_N)_1$H/2 + $(g_N\beta_N)_2$H/2

A(4,2) = $\sqrt{3}$*Q4/2

A(9,2) = Q6

A(10,2) = Q1 - Q7/2 + 3*Q4/2

A(12,2) = $\sqrt{3}$*Q2

A(3,3) = W3/2 + W9/4 + W15/4 - $(g_N\beta_N)_1$H/2 - $(g_N\beta_N)_2$H/2

A(4,3) = Q7/2

A(5,3) = Q4

A(9,3) = $-\sqrt{3}$*Q3

A(11,3) = Q1 + Q4/2 + Q7/2

A(12,3) = Q5

A(13,3) = 2*Q2

A(4,4) = W3/2 + W9/4 - W15/4 - $(g_N\beta_N)_1$H/2 + $(g_N\beta_N)_2$H/2

A(6,4) = Q4

A(10,4) = $-\sqrt{3}$*Q3

A(11,4) = Q6

A(12,4) = Q1 + Q4/2 - Q7/2

A(14,4) = 2*Q2

A(5,5) = W3/2 - W9/4 + W15/4 + $(g_N\beta_N)_1$H/2 - $(g_N\beta_N)_2$H/2

A(6,5) = Q7/2

A(7,5) = $-\sqrt{3}$*Q4/2

A(11,5) = 2*Q3

A(13,5) = Q1 - Q4/2 + Q7/2

A(14,5) = Q5

A(15,5) = $-\sqrt{3}$*Q2

A(6,6) = W3/2 - W9/4 - W15/4 + $(g_N\beta_N)_1$H/2 + $(g_N\beta_N)_2$H/2

A(8,6) = $-\sqrt{3}$*Q4/2

A(12,6) = 2*Q3

A(13,6) = Q6

A(14,6) = Q1 - Q4/2 - Q7/2

A(16,6) = $-\sqrt{3}$*Q2

A(7,7) = W3/2 - 3*W9/4 + W15/4 + 3*$(g_N\beta_N)_1$H/2 - $(g_N\beta_N)_2$H/2

A(8,7) = Q7/2

$A(13,7) = \sqrt{3}*Q3$

$A(15,7) = Q1 - 3*Q4/2 + Q7/2$

$A(16,7) = Q5$

$A(8,8) = W3/2 - 3*W9/4 - W15/4 + 3*(g_N\beta_N)_1H/2 + (g_N\beta_N)_2H/2$

$A(14,8) = \sqrt{3}*Q3$

$A(15,8) = Q6$

$A(16,8) = Q1 - 3*Q4/2 - Q7/2$

$A(9,9) = -W3/2 - 3*W9/4 - W15/4 - 3*(g_N\beta_N)_1H/2 - (g_N\beta_N)_2H/2$

$A(10,9) = -Q7/2$

$A(11,9) = \sqrt{3}*Q4/2$

$A(10,10) = -W3/2 - 3*W9/4 + W15/4 - 3*(g_N\beta_N)_1H/2 + (g_N\beta_N)_2H/2$

$A(12,10) = \sqrt{3}*Q4/2$

$A(11,11) = -W3/2 - W9/4 - W15/4 - (g_N\beta_N)_1H/2 - (g_N\beta_N)_2H/2$

$A(12,11) = -Q7/2$

$A(13,11) = -Q4$

$A(12,12) = -W3/2 - W9/4 + W15/4 - (g_N\beta_N)_1H/2 + (g_N\beta_N)_2H/2$

$A(14,12) = -Q4$

$A(13,13) = -W3/2 + W9/4 - W15/4 + (g_N\beta_N)_1H/2 - (g_N\beta_N)_2H/2$

$A14,13) = -Q7/2$

$A(15,13) = \sqrt{3}*Q4/2$

$A(14,14) = -W3/2 + 3*W9/4 - W15/4 + 3*(g_N\beta_N)_1H/2 - (g_N\beta_N)_2H/2$

$A(16,14) = \sqrt{3}*Q4/2$

$A(15,15) = -W3/2 + 3*W9/4 - W15/4 + 3*(g_N\beta_N)_1H/2 - (g_N\beta_N)_2H/2$

$A16,15) = -Q7/2$

$A(16,16) = -W3/2 + 3*W9/4 + W15/4 + 3*(g_N\beta_N)_1H/2 + (g_N\beta_N)_2H/2$

TABLE I

LOWER HALF OF THE SPIN HAMILTONIAN MATRIX

	|a,c,a>	|a,c,b>	|a,a,a>	|a,a,b>	|a,b,a>	|a,b,b>	|a,d,a>	|a,d,b>	|b,c,a>	|b,c,b>	|b,a,a>	|b,a,b>	|b,b,a>	|b,b,b>	|b,d,a>	|b,d,b> [a]
|a,c,a>	A(1,1)															
|a,c,b>	A(2,1)	A(2,2)														
|a,a,a>	A(3,1)	0	A(3,3)													
|a,a,b>	0	A(4,2)	A(4,3)	A(4,4)												
|a,b,a>	0	0	A(5,3)	0	A(5,5)											
|a,b,b>	0	0	0	A(6,4)	A(6,5)	A(6,6)										
|a,d,a>	0	0	0	0	A(7,5)	0	A(7,7)									
|a,d,b>	0	0	0	0	0	A(8,6)	A(8,7)	A(8,8)								
|b,c,a>	A(9,1)	A(9,2)	A(9,3)	0	0	0	0	0	A(9,9)							
|b,c,b>	A(10,1)	A(10,2)	0	A(10,4)	0	0	0	0	A(10,9)	A(10,10)						
|b,a,a>	A(11,1)	0	A(11,3)	A(11,4)	A(11,5)	0	0	0	A(11,9)	0	A(11,11)					
|b,a,b>	0	A(12,2)	A(12,3)	A(12,4)	0	A(12,6)	0	0	0	A(12,10)	A(12,11)	A(12,12)				
|b,b,a>	0	0	A(13,3)	0	A(13,5)	A(13,6)	A(13,7)	0	0	0	A(13,11)	0	A(13,13)			
|b,b,b>	0	0	0	A(14,4)	A(14,5)	A(14,6)	0	A(14,8)	0	0	0	A(14,12)	A(14,13)	A(14,14)		
|b,d,a>	0	0	0	0	A(15,5)	0	A(15,7)	A(15,8)	0	0	0	0	A(15,13)	0	A(15,15)	
|b,d,b>	0	0	0	0	0	A(16,6)	A(16,7)	A(16,8)	0	0	0	0	0	A(16,14)	A(16,15)	A(16,16)

[a]Notation is a=1/2, b=-1/2, c=3/2, and d=-3/2.

CHAPTER IV

EXPERIMENTAL RESULTS AND ANALYSIS

When the synthetic quartz ESR sample was irradiated at 200 K and then irradiated again at 77 K, the $[SiO_4/Li]^o$ center was created. Figure 5 shows the ESR spectrum of the aluminum-hole center and the central portion of the $[SiO_4/Li]^o$ center after irradiation. The magnetic field was parallel to the crystal's c-axis and the measurement temperature was 77 K. The aluminum-hole center provided the easiest way to assure that the c-axis of the sample was aligned with the magnetic field . The spectrometer's lock-in amplifier was then set "out of phase" to better observe the $[SiO_4/Li]^o$ center spectrum. This is required beause of the long spin-lattice relaxation time associated with this defect. The $[SiO_4/Li]^o$ center ESR spectrum contains four equally intense lines that were 0.9 gauss apart. An enlarged view of this spectrum is shown in figure 6. The angular dependence of this spectrum has been reported by Jani et al. [9]. In addition to the g and A tensor parameters, these investigators used the electron-nuclear double resonance technique to prove ^7Li was the responsible nucleus for the hyperfine interaction.

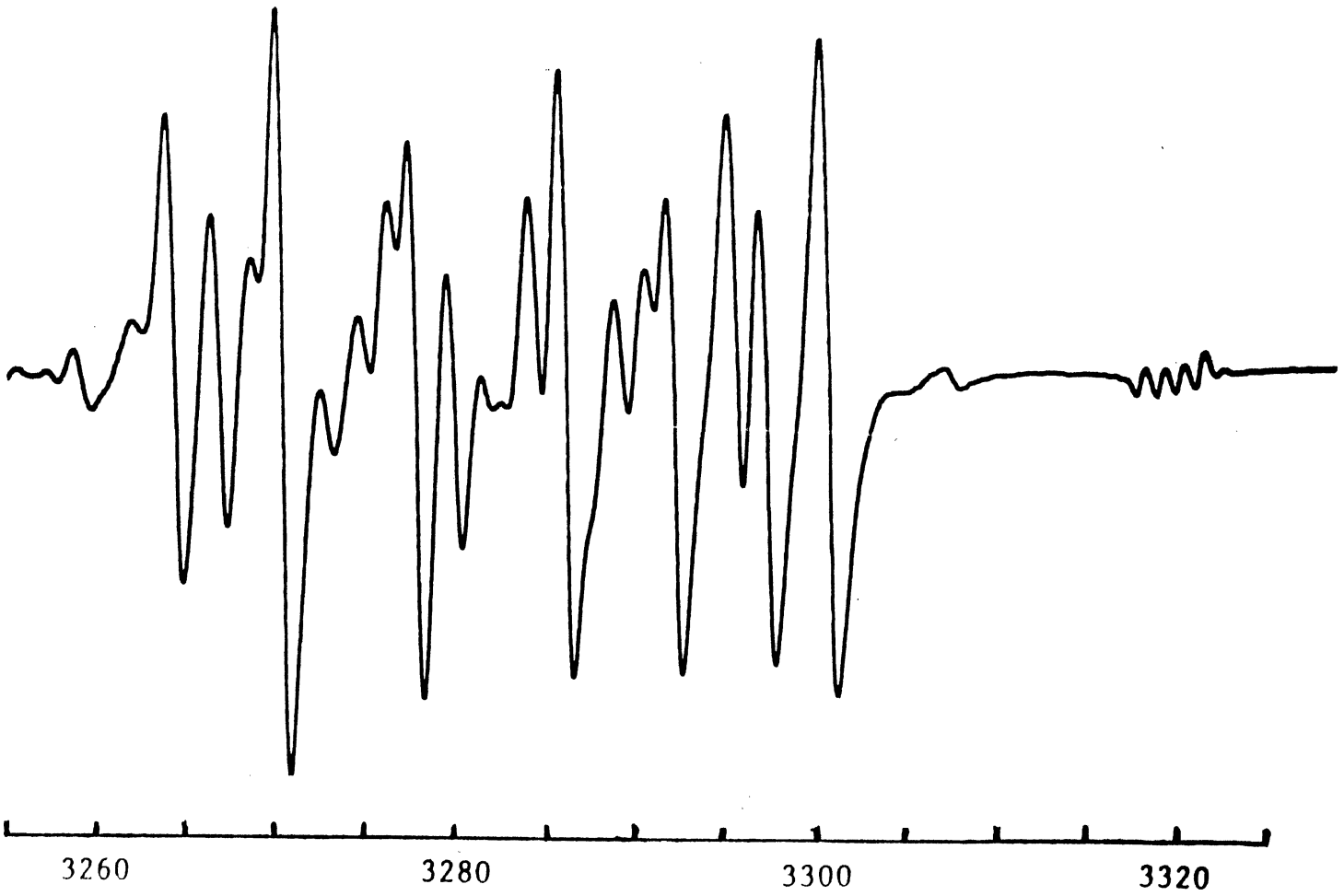

Figure 5. ESR Spectrum of the $[AlO_4]^o$ Center and the $[SiO_4/Li]^o$ Center Lines

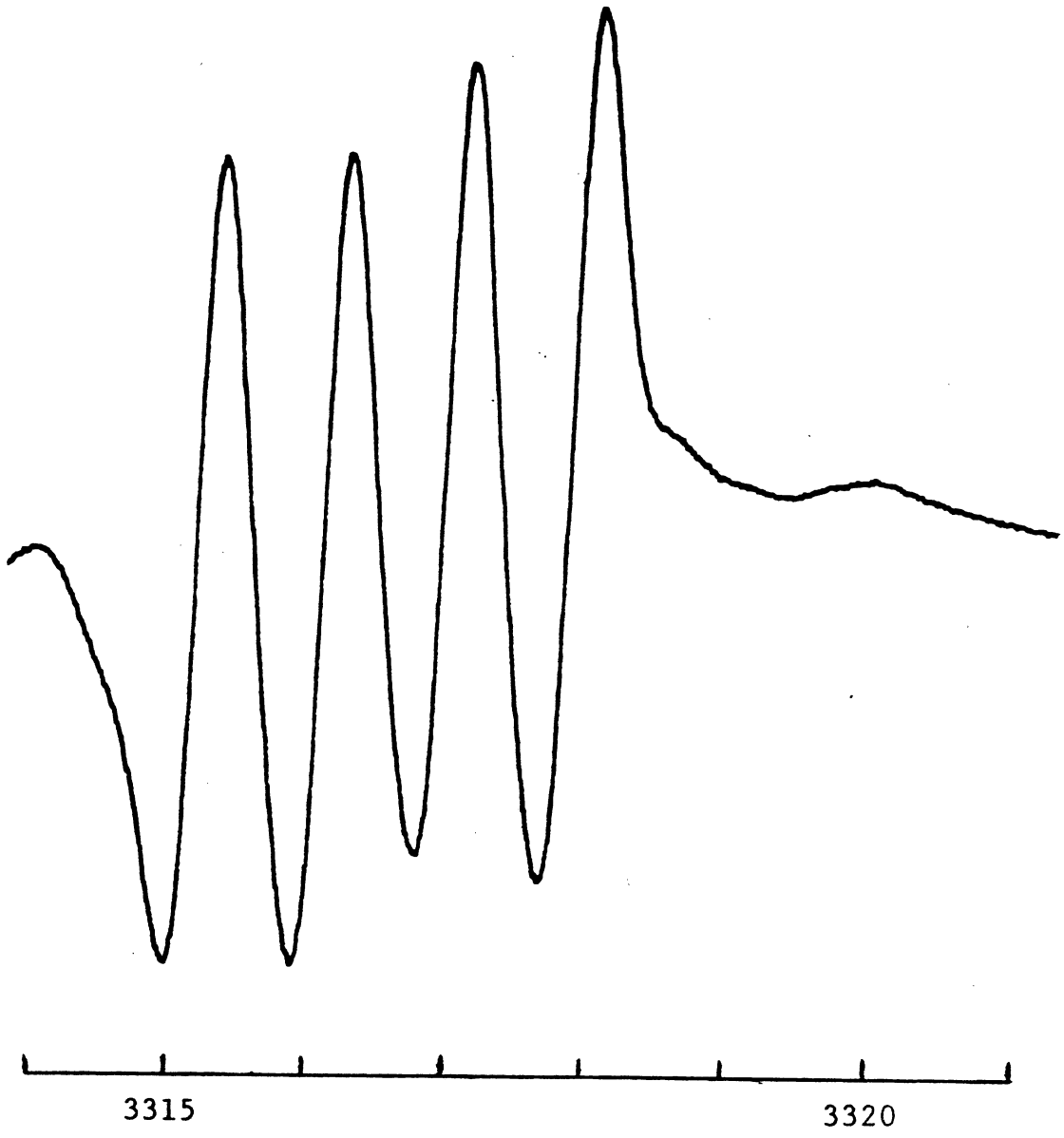

Figure 6. Enlargement of $[SiO_4/Li]^0$ Center Line Spectrum

In addition to the lithium hyperfine spectrum, there are eight lines arising from a ^{29}Si hyperfine interaction. Four of these lines are about 216 gauss below the lithium hyperfine spectrum and the other four are about 190 gauss above the lithium hyperfine spectrum. A c-axis spectrum of these high field lines and the low field lines is shown in figure 7.

An angular dependence study of these high and low field lines was carried out at 77 K. The magnetic field was rotated in the plane perpendicular to the X-axis (or twofold axis) and spectra were taken at 10 degree intervals, with the exception of two 15 degree intevals on the negative angle side. The data was taken for angles up to 70 degrees on either side of the zero angle (corresponding to the c-axis). We were not able to rotate the magnet to greater angles wthout the faces of the magnet striking the cavity. The results of the angular dependence study are presented in figure 8. The angular dependence of both high and low fields is shown.

Usually, rotation of the magnetic field in this plane will cause each line in the spectrum to split into three lines. This is because of the symmetry of the quartz lattice. In the case of the $[SiO_4/Li]^o$ center, however, the lines only split into two components when the magnetic field was rotated in the plane perpendicular to the X-axis. One component is roughly twice as large as the other, indicating that the large one is doubly degenerate. This degeneracy

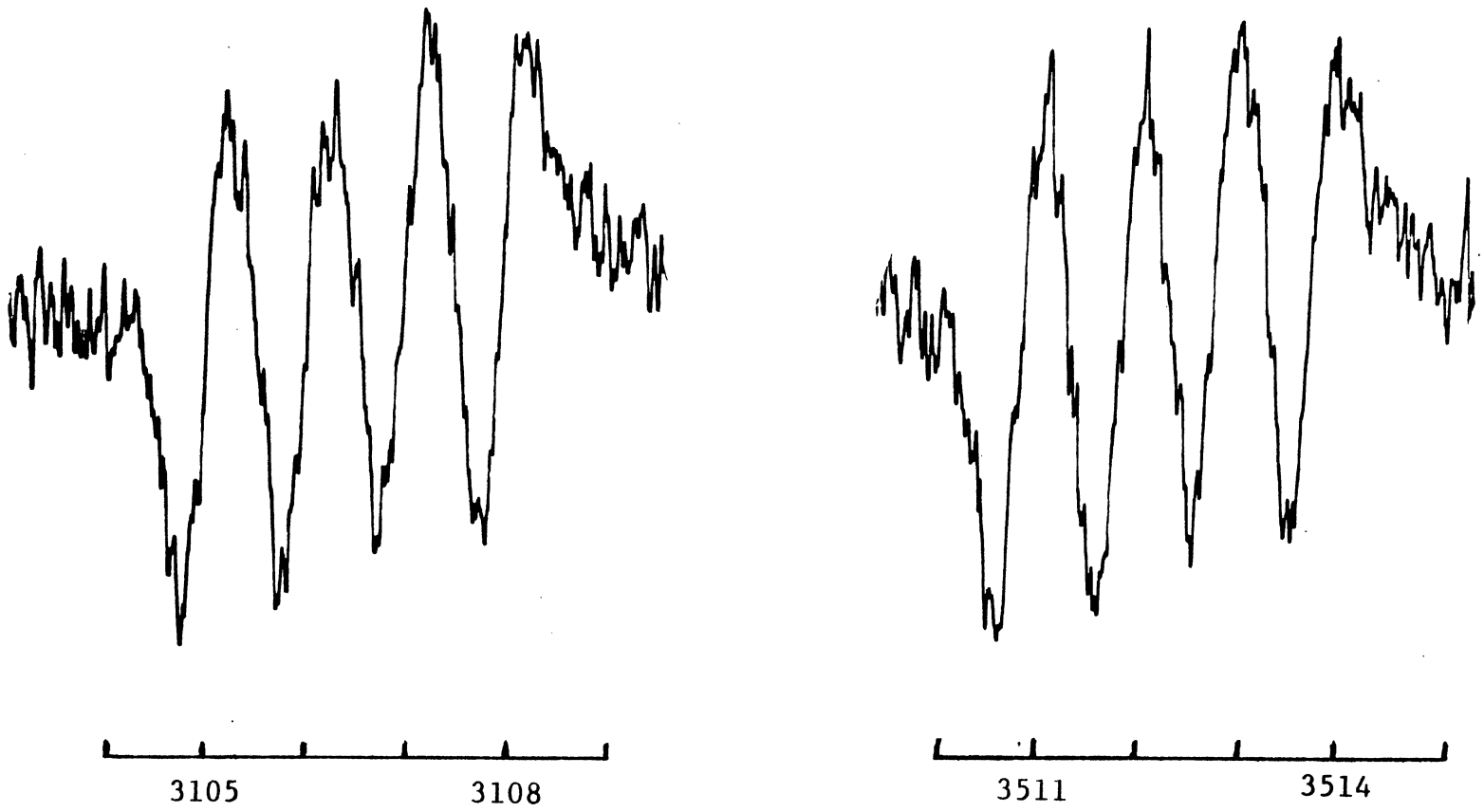

Figure 7. ESR Spectrum of High and Low Field Regions of the $[SiO_4/Li]^o$ Center

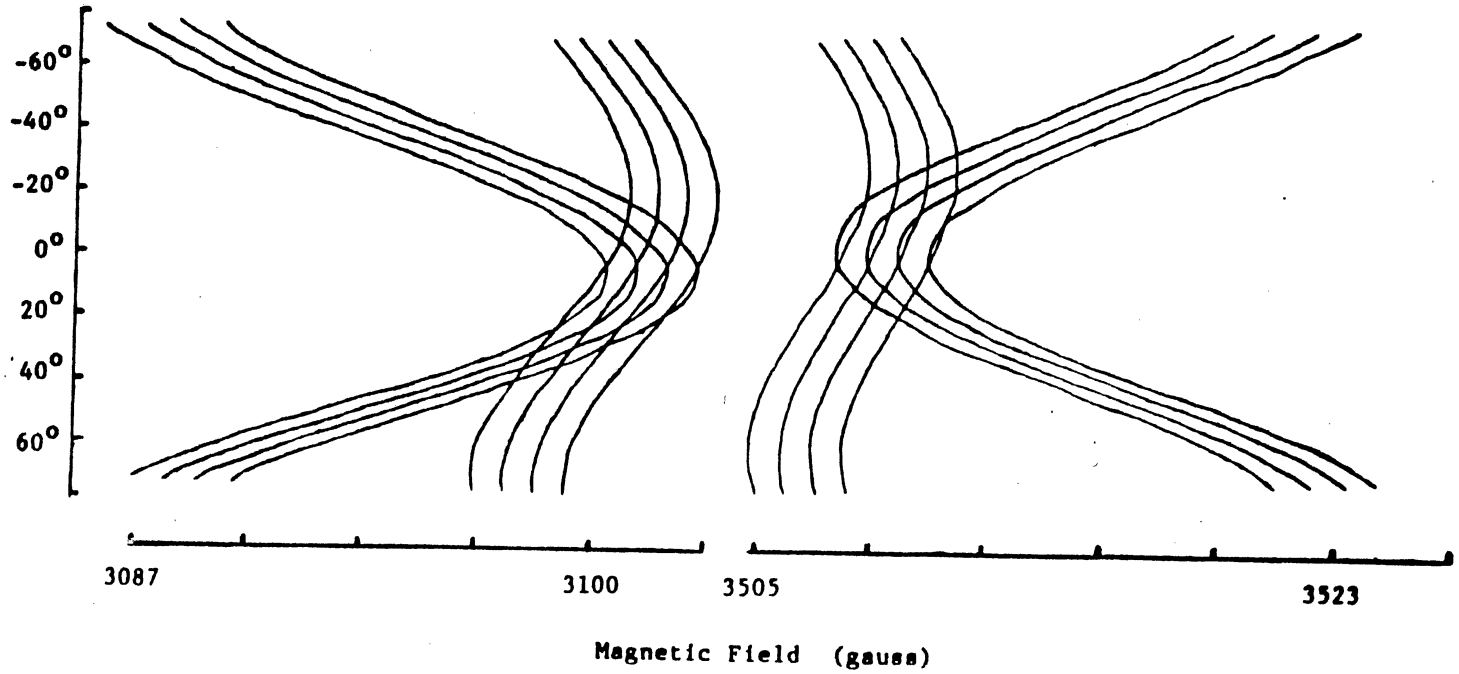

Figure 8. Angular Dependence Study of Lines in High and Low Field Regions

means that the $[SiO_4/Li]^o$ center is symmetrical about one of the twofold axes of the crystal, which, in turn, means that the lithium ion lies on the axis passing through the adjacent silicon ions.

To assure that our convention for positive and negative angles was correct, the E_1' center was produced (in accordance with Jani et al. [13]) in the same sample and the ESR spectra were taken at plus and minus 30 degrees to see if the negative and positive angles for the E_1' center agreed with our negative and positive angles we had assumed when the crystal was in the same orientation. A notch was made on the top of the sample to assure that it was placed in the Dewar in the same orientation each time.

The matrix elements from the theoretical analysis were placed into two computer programs to analyze the experimental data. The first program, a listing of which is given in Appendix A, is a line-position program. Given a specific set of spin Hamiltonian parameters and a given microwave frequency, this program calculates the values of the magnetic fields at which the ESR lines will appear. For each angle, there will be eight possible energy transitions according to the selection rules $\Delta M = \pm 1$, $\Delta m_1 = 0$, and $\Delta m_2 = 0$. These transitions are listed below in terms of the energy eigenvalues D(I). Figure 9 shows the energy levels and the possible transitions.

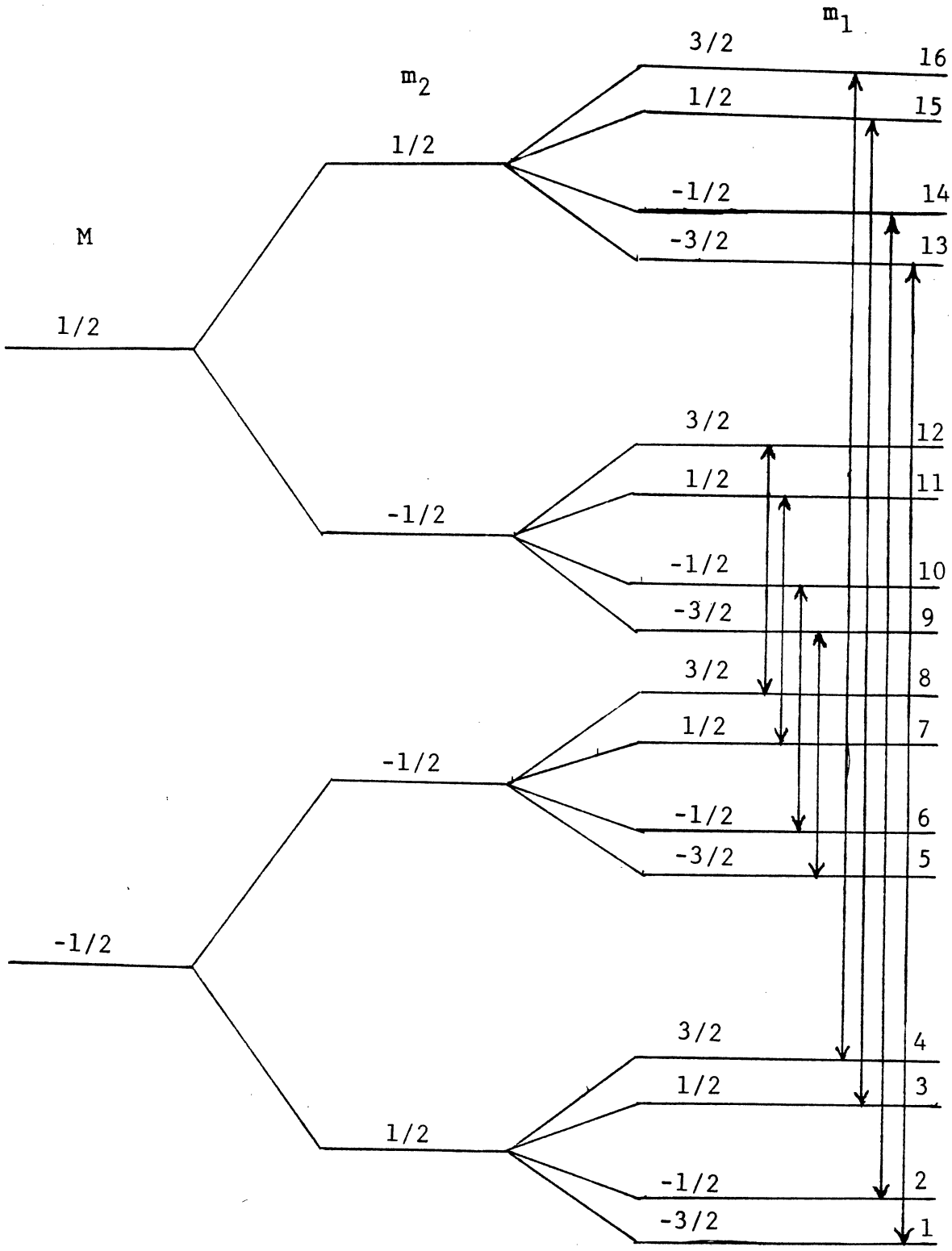

Figure 9. Energy Level Diagram of S=1/2, I_1=3/2, and I_2=1/2 System

$h\nu_1$=D(13)-D(1)

$h\nu_2$=D(14)-D(2)

$h\nu_3$=D(15)-D(3)

$h\nu_4$=D(16)-D(4)

$h\nu_5$=D(9)-D(5)

$h\nu_6$=D(10)-D(6)

$h\nu_7$=D(11)-D(7)

$h\nu_8$=D(12)-D(8)

To actually determine a specific line position, the field value was systematically varied and the microwave frequency recalculated at each step until the difference between the calculated and experimental microwave frequency had become less than a specified value. When this condition was met, the last value of the field was taken as the calculated magnetic field.

The second program (listed in Appendix B), which is a matrix fitting program, calculates what the final set of parameters for the g and A tensors should be using the measured line positions and corresponding microwave frequencies for each of the angles investigated. Each line is given an I and K value, corresponding to which of the eight transitions it represents and to which of the three magnetically inequivalent orientations it represents, respectively. Each of the 306 data points inputed to the program then consists of the magnetic field strength, the microwave frequency, and an I and K value. The set of parameters in the fitting program are systematically varied until a good agreement

between the calculated and the experimental values of the magnetic field positions is obtained. The microwave frequency for each magnetic field value is calculated and then compared to the experimental value of the microwave frequency for that field value. The quantity SUM is calculated by

$$\text{SUM} = \sum_{i=1}^{306} \left[\nu_i^{exp} - \nu_i^{cal} \right]^2$$

One of the parameters is then increased by a specified amount and a new set of microwave frequencies and a new SUM are then calculated. If the new SUM is smaller than the old SUM, then this process is continued; if not, then the parameter is decreased and the two SUMs compared. This procedure is repeated for all the spin Hamiltonian parameters. When the program finds a set of parameters for which any change in any parameter fails to lower the value of SUM, the iteration process is complete and the final set of parameters are reported. The set of final parameters is given in table II. This final set of parameters obtained from the fitting program is the set of parameters then used in the line position program to obtain the calculated magnetic field values plotted in figure 8.

TABLE II

SPIN HAMILTONIAN FINAL PARAMETERS

	Principal Values (MHz)	Principal Directions[a]
g_x	2.0007	(85^o, 0^o)
g_y	2.0017	(65^o, 90^o)
g_z	1.9990	(25^o, 265^o)
A_{1x}	2.49	(0^o, 270^o)
A_{1y}	2.75	(90^o, 90^o)
A_{1z}	4.11	(90^o, 0^o)
A_{2x}	-1135	(0^o, 270^o)
A_{2y}	-1130	(90^o, 90^o)
A_{2z}	-1250	(90^o, 0^o)

[a] In accordance with Jani et al. [9].

CHAPTER V

DISCUSSION

In this study, I have continued an ongoing analysis of the electronic structure of the $[SiO_4/Li]^o$ center. Specifically, I have conducted an angular dependence study of the ESR spectrum associated with the strong silicon hyperfine interaction. Taking this data and using it in a computer program, I have calculated the principal values and the principal-axis directions of the ^{29}Si A tensor. The "best" values for these parameters were reported in the previous chapter. A physical interpretation of these spin-Hamiltonian parameters reveals that the ^{29}Si hyperfine interaction has its principal direction exactly along the crystal's twofold axis and thus verified the high-symmetry on-axis location of the lithium atom in this defect.

Further studies of this particular point defect in quartz should consist of an ENDOR investigation to obtain the data necessary for calculations of the nuclear electric quadrupole interaction of the lithium nucleus in the $[SiO_4/Li]^o$ center.

Another possible avenue of study would consist of an ESR study of the $[SiO_4/Na]^o$ center, which appears to be

similar in nature to the $[SiO_4/Li]^0$ center. A preliminary investigation of a sodium-electrodiffused sample showed that the ESR spectrum at 77 K was not well defined. This suggests the possibility that the defect has a high-frequency reorientation between equivalent sites similar to the behavior of the $[AlO_4/Na]^0$ center in acoustic loss experiments. Therefore, ESR data would have to be taken at liquid-helium temperatures. This ESR data, once found, could then be correlated to the thermoluminescence study performed by Halperin and Katz [12] in the same way that Halperin, Jani, and Halliburton [10] compared the TSL and ESR data of the $[SiO_4/Li]^0$ center. Such an investigation may help determine more exactly how these two defect centers are related.

A SELECTED BIBLIOGRAPHY

1. Halliburton, L. E., J. J. Martin, and D. R. Koehler, in Precision Frequency Control, (Academic Press, New York, 1985), Vol. 1, Chapter 1.

2. Halliburton, L. E., Cryst. Latt. Def. 12, 163 (1985).

3. Weil, J. A., Phys. Chem. Miner. 10, 149 (1984).

4. King, J. C., Bell Syst. Tech. J. 38, 573 (1959).

5. Fraser, D. B., J. Appl. Phys. 35, 2913 (1964).

6. Stevels, J. M., and J. Volger, Philips Res. Rep. 17, 283 (1962).

7. Nowick, A. S., and M. W. Stanley, J. Appl. Phys. 40, 4995 (1969).

8. Toulouse, J., E. R. Green, and A. S. Nowick, in Proceedings of the 37th Annual Symposium on Frequency Control, p. 125 (1983).

9. Jani, M. G., L. E. Halliburton, and A. Halperin, Phys. Rev. Lett. 56, 1392 (1986).

10. Halperin, A., M. G. Jani, and L. E. Halliburton, Phys. Rev. B 34, 5702 (1986).

11. Wilson, T. M., J. A. Weil, and P. S. Rao, Phys. Rev. B 34, 6053 (1986).

12. Halperin, A., and S. Katz, Solid State Commun. 63, 697 (1987).

13. Jani, M. G., R. B. Bossoli, and L. E. Halliburton, Phys. Rev. B 27, 2285 (1983).

APPENDIX A

```
10    REM        ******* [SiO4/Li] LINE POSITION *******
20    REM
30    DEG
40    OPTION BASE 1
50    DIM P(18),Hf(8),G(3,3),H(3,3),Rm(3,3),R2(3,3),R3(3,3)
51    DIM Rt(3,3),R(3,3)
60    DIM Tg(3,3),Th(3,3),B(3,3),Tb(3,3)
70    DIM Ar(16,16),Ai(16,16),D(16),E(16),E2(16),Tau(2,16)
80    INTEGER I,J,K,L,M,N
90    PRINTER IS 701
100   P(1)=2.0007
110   P(2)=2.0017
120   P(3)=1.999
130   P(4)=25
140   P(5)=-5
150   P(6)=5
160   P(7)=2.49
170   P(8)=2.75
180   P(9)=4.11
190   P(10)=-90
200   P(11)=-90
210   P(12)=-55
220   P(13)=-1135.02
230   P(14)=-1129.53
240   P(15)=-1249.72
250   P(16)=90
260   P(17)=-90
270   P(18)=-20
280   PRINT "/"
290   PRINT P(*);
300   PRINT "/"
310   N=16
320   Nm=16
330   Bl=9.2741/6.6262
340   Gbn1=1.6547E-3
350   Gbn2=8.458E-4
360   Freqq=9299.076
370   Allpha=0
380   Beta=-90
390   Ag=SIN(P(4))
400   Aag=COS(P(4))
410   Cg=SIN(P(5))
420   Ccg=COS(P(5))
430   Fg=SIN(P(6))
440   Ffg=COS(P(6))
450   Ah=SIN(P(10))
460   Aah=COS(P(10))
470   Ch=SIN(P(11))
480   Cch=COS(P(11))
490   Fh=SIN(P(12))
500   Ffh=COS(P(12))
510   Ab=SIN(P(16))
520   Aab=COS(P(16))
530   Cb=SIN(P(17))
540   Ccb=COS(P(17))
550   Fb=SIN(P(18))
560   Ffb=COS(P(18))
570   G(1,1)=Ffg*Ccg-Aag*Cg*Fg
580   G(1,2)=Ffg*Cg+Aag*Ccg*Fg
590   G(1,3)=Fg*Ag
```

```
600   G(2,1)=-(Fg*Ccg)-Aag*Cg*Ffg
610   G(2,2)=-(Fg*Cg)+Aag*Ccg*Ffg
620   G(2,3)=-Ffg*Ag
630   G(3,1)=-Ag*Cg
640   G(3,2)=-(Ag*Ccg)
650   G(3,3)=-Aag
660   H(1,1)=-Ffh*Cch-Aah*Ch*Fh
670   H(1,2)=-Ffh*Ch+Aah*Cch*Fh
680   H(1,3)=-Fh*Ah
690   H(2,1)=-(Fh*Cch)-Aah*Ch*Ffh
700   H(2,2)=-(Fh*Ch)+Aah*Cch*Ffh
710   H(2,3)=Ffh*Ah
720   H(3,1)=Ah*Ch
730   H(3,2)=-(Ah*Cch)
740   H(3,3)=Aah
750   B(1,1)=Ffb*Ccb-Aab*Cb*Fb
760   B(1,2)=Ffb*Cb+Aab*Ccb*Fb
770   B(1,3)=Fb*Ab
780   B(2,1)=-(Fb*Ccb)-Aab*Cb*Ffb
790   B(2,2)=-(Fb*Cb)+Aab*Ccb*Ffb
800   B(2,3)=Ffb*Ab
810   B(3,1)=Ab*Cb
820   B(3,2)=-Ab*Ccb
830   B(3,3)=Aab
840   PRINT "/"
850   PRINT Allpha,Beta
860   Rm(1,1)=COS(Allpha)
870   Rm(1,2)=-(SIN(Allpha)*SIN(Beta))
880   Rm(1,3)=SIN(Allpha)*COS(Beta)
890   Rm(2,1)=0
900   Rm(2,2)=COS(Beta)
910   Rm(2,3)=SIN(Beta)
920   Rm(3,1)=-SIN(Allpha)
930   Rm(3,2)=-(COS(Allpha)*SIN(Beta))
940   Rm(3,3)=COS(Allpha)*COS(Beta)
950   K=1
960   ON K GOTO 970,970,970,990,990,990
970   MAT R2= IDN
980   ON K GOTO 1040,1060,1120
990   MAT R2= IDN
1000  R2(2,2)=-1
1010  R2(3,3)=-1
1020  Kk=K-3
1030  ON Kk GOTO 1040,1060,1120
1040  MAT R3= IDN
1050  GOTO 1170
1060  MAT R3= IDN
1070  R3(1,1)=COS(120)
1080  R3(1,2)=SIN(120)
1090  R3(2,1)=-SIN(120)
1100  R3(2,2)=COS(120)
1110  GOTO 1170
1120  MAT R3= IDN
1130  R3(1,1)=COS(120)
1140  R3(1,2)=-SIN(120)
1150  R3(2,1)=SIN(120)
1160  R3(2,2)=COS(120)
1170  MAT Rt= R2*R3
1180  MAT R= Rt*Rm
1190  MAT Tg= G*R
```

```
1200  MAT Th= H*R
1210  MAT Tb= B*R
1220  Ic=1
1230  Hh=3300
1231  O1=P(3)*Tg(3,1)*Tg(3,3)
1240  W1=B1*Hh*(P(1)*Tg(1,1)*Tg(1,3)+P(2)*Tg(2,1)*Tg(2,3)+O1)
1241  O2=P(3)*Tg(3,2)*Tg(3,3)
1250  W2=B1*Hh*(P(1)*Tg(1,2)*Tg(1,3)+P(2)*Tg(2,2)*Tg(2,3)+O2)
1251  O3=P(3)*Tg(3,3)*Tg(3,3)
1260  W3=B1*Hh*(P(1)*Tg(1,3)*Tg(1,3)+P(2)*Tg(2,3)*Tg(2,3)+O3)
1261  O4=P(9)*Th(3,1)*Th(3,1)
1270  W4=P(7)*Th(1,1)*Th(1,1)+P(8)*Th(2,1)*Th(2,1)+O4
1271  O5=P(9)*Th(3,1)*Th(3,2)
1280  W5=P(7)*Th(1,1)*Th(1,2)+P(8)*Th(2,1)*Th(2,2)+O5
1281  O6=P(9)*Th(3,1)*Th(3,3)
1290  W6=P(7)*Th(1,1)*Th(1,3)+P(8)*Th(2,1)*Th(2,3)+O6
1291  O7=P(9)*Th(3,2)*Th(3,2)
1300  W7=P(7)*Th(1,2)*Th(1,2)+P(8)*Th(2,2)*Th(2,2)+O7
1301  O8=P(9)*Th(3,2)*Th(3,3)
1310  W8=P(7)*Th(1,2)*Th(1,3)+P(8)*Th(2,2)*Th(2,3)+O8
1311  O9=P(9)*Th(3,3)*Th(3,3)
1320  W9=P(7)*Th(1,3)*Th(1,3)+P(8)*Th(2,3)*Th(2,3)+O9
1321  O10=P(15)*Tb(3,1)*Tb(3,1)
1330  W10=P(13)*Tb(1,1)*Tb(1,1)+P(14)*Tb(2,1)*Tb(2,1)+O10
1331  O11=P(15)*Tb(3,1)*Tb(3,2)
1340  W11=P(13)*Tb(1,1)*Tb(1,2)+P(14)*Tb(2,1)*Tb(2,2)+O11
1341  O12=P(15)*Tb(3,1)*Tb(3,3)
1350  W12=P(13)*Tb(1,1)*Tb(1,3)+P(14)*Tb(2,1)*Tb(2,3)+O12
1351  O13=P(15)*Tb(3,2)*Tb(3,2)
1360  W13=P(13)*Tb(1,2)*Tb(1,2)+P(14)*Tb(2,2)*Tb(2,2)+O13
1361  O14=P(15)*Tb(3,2)*Tb(3,3)
1370  W14=P(13)*Tb(1,2)*Tb(1,3)+P(14)*Tb(2,2)*Tb(2,3)+O14
1371  O15=P(15)*Tb(3,3)*Tb(3,3)
1380  W15=P(13)*Tb(1,3)*Tb(1,3)+P(14)*Tb(2,3)*Tb(2,3)+O15
1390  Q1r=W1/2
1400  Q1i=W2/2
1410  Q2r=(W4-W7)/4
1420  Q2i=W5/2
1430  Q3=(W4+W7)/4
1440  Q4r=W6/2
1450  Q4i=W8/2
1460  Q5r=(W10-W13)/4
1470  Q5i=W11/2
1480  Q6=(W10+W13)/4
1490  Q7r=W12/2
1500  Q7i=W14/2
1510  FOR I=1 TO 16
1520  FOR J=1 TO 16
1530  Ar(I,J)=0
1540  Ai(I,J)=0
1550  NEXT J
1560  NEXT I
1570  Ar(1,1)=W3/2+3*W9/4+W15/4-3*Gbn1*Hh/2-Gbn2*Hh/2
1580  Ar(2,2)=W3/2+3*W9/4-W15/4-3*Gbn1*Hh/2+Gbn2*Hh/2
1590  Ar(3,3)=W3/2+W9/4+W15/4-Gbn1*Hh/2-Gbn2*Hh/2
1600  Ar(4,4)=W3/2+W9/4-W15/4-Gbn1*Hh/2+Gbn2*Hh/2
1610  Ar(5,5)=W3/2-W9/4+W15/4+Gbn1*Hh/2-Gbn2*Hh/2
1620  Ar(6,6)=W3/2-W9/4-W15/4+Gbn1*Hh/2+Gbn2*Hh/2
1630  Ar(7,7)=W3/2-3*W9/4+W15/4+3*Gbn1*Hh/2-Gbn2*Hh/2
1640  Ar(8,8)=W3/2-3*W9/4-W15/4+3*Gbn1*Hh/2+Gbn2*Hh/2
```

```
1650  Ar(9,9)=-W3/2-3*W9/4-W15/4-3*Gbn1*Hh/2-Gbn2*Hh/2
1660  Ar(10,10)=-W3/2-3*W9/4+W15/4-3*Gbn1*Hh/2+Gbn2*Hh/2
1670  Ar(11,11)=-W3/2-W9/4-W15/4-Gbn1*Hh/2-Gbn2*Hh/2
1680  Ar(12,12)=-W3/2-W9/4+W15/4-Gbn1*Hh/2+Gbn2*Hh/2
1690  Ar(13,13)=-W3/2+W9/4-W15/4+Gbn1*Hh/2-Gbn2*Hh/2
1700  Ar(14,14)=-W3/2+W9/4+W15/4+Gbn1*Hh/2+Gbn2*Hh/2
1710  Ar(15,15)=-W3/2+3*W9/4-W15/4+3*Gbn1*Hh/2-Gbn2*Hh/2
1720  Ar(16,16)=-W3/2+3*W9/4+W15/4+3*Gbn1*Hh/2+Gbn2*Hh/2
1730  Ar(2,1)=Q7r/2
1740  Ai(2,1)=Q7i/2
1750  Ar(3,1)=SQR(3)*Q4r/2
1760  Ai(3,1)=SQR(3)*Q4i/2
1770  Ar(9,1)=Q1r+3*Q4r/2+Q7r/2
1780  Ai(9,1)=Q1i+3*Q4i/2+Q7i/2
1790  Ar(10,1)=Q5r
1800  Ai(10,1)=Q5i
1810  Ar(11,1)=SQR(3)*Q2r
1820  Ai(11,1)=SQR(3)*Q2i
1830  Ar(4,2)=SQR(3)*Q4r/2
1840  Ai(4,2)=SQR(3)*Q4i/2
1850  Ar(9,2)=Q6
1860  Ar(10,2)=Q1r-Q7r/2+3*Q4r/2
1870  Ai(10,2)=Q1i-Q7i/2+3*Q4i/2
1880  Ar(12,2)=SQR(3)*Q2r
1890  Ai(12,2)=SQR(3)*Q2i
1900  Ar(4,3)=Q7r/2
1910  Ai(4,3)=Q7i/2
1920  Ar(5,3)=Q4r
1930  Ai(5,3)=Q4i
1940  Ar(9,3)=SQR(3)*Q3
1950  Ar(11,3)=Q1r+Q4r/2+Q7r/2
1960  Ai(11,3)=Q1i+Q4i/4+Q7i/2
1970  Ar(12,3)=Q5r
1980  Ai(12,3)=Q5i
1990  Ar(13,3)=Q2r*2
2000  Ai(13,3)=Q2i*2
2010  Ar(6,4)=Q4r
2020  Ai(6,4)=Q4i
2030  Ar(10,4)=SQR(3)*Q3
2040  Ar(11,4)=Q6
2050  Ar(12,4)=Q1r+Q4r/2-Q7r/2
2060  Ai(12,4)=Q1i+Q4i/2-Q7i/2
2070  Ar(14,4)=Q2r*2
2080  Ai(14,4)=Q2i*2
2090  Ar(6,5)=Q7r/2
2100  Ai(6,5)=Q7i/2
2110  Ar(7,5)=SQR(3)*Q4r/2
2120  Ai(7,5)=SQR(3)*Q4i/2
2130  Ar(11,5)=Q3*2
2140  Ar(13,5)=Q1r-Q4r/2+Q7r/2
2150  Ai(13,5)=Q1i-Q5i/2+Q7i/2
2160  Ar(14,5)=Q5r
2170  Ai(14,5)=Q5i
2180  Ar(15,5)=SQR(3)*Q2r
2190  Ai(15,5)=SQR(3)*Q2i
2200  Ar(8,6)=SQR(3)*Q4r/2
2210  Ai(8,6)=SQR(3)*Q4i/2
2220  Ar(12,6)=2*Q3
2230  Ar(13,6)=Q6
2240  Ar(14,6)=Q1r-Q4r/2-Q7r/2
```

```
2250  Ai(14,6)=Q1i-Q4i/2-Q7i/2
2260  Ar(16,6)=SQR(3)*Q2r
2270  Ai(16,6)=SQR(3)*Q2i
2280  Ar(8,7)=Q7r/2
2290  Ai(8,7)=Q7i/2
2300  Ar(13,7)=SQR(3)*Q3
2310  Ar(15,7)=Q1r-3*Q4r/2+Q7r/2
2320  Ai(15,7)=Q1i-3*Q4i/2+Q7i/2
2330  Ar(16,7)=Q5r
2340  Ai(16,7)=Q5i
2350  Ar(14,8)=SQR(3)*Q3
2360  Ar(15,8)=Q6
2370  Ar(16,8)=Q1r-3*Q4r/2-Q7r/2
2380  Ai(16,8)=Q1i-3*Q4i/2-Q7i/2
2390  Ar(10,9)=-Q7r/2
2400  Ai(10,9)=-Q7i/2
2410  Ar(11,9)=-SQR(3)*Q4r/2
2420  Ai(11,9)=-SQR(3)*Q4i/2
2430  Ar(12,10)=-SQR(3)*Q4r/2
2440  Ai(12,10)=-SQR(3)*Q4i/2
2450  Ar(12,11)=-Q7r/2
2460  Ai(12,11)=-Q7i/2
2470  Ar(13,11)=-Q4r
2480  Ai(13,11)=-Q4i
2490  Ar(14,12)=-Q4r
2500  Ai(14,12)=-Q4i
2510  Ar(14,13)=-Q7r/2
2520  Ai(14,13)=-Q7i/2
2530  Ar(15,13)=-SQR(3)*Q4r/2
2540  Ai(15,13)=-SQR(3)*Q4i/2
2550  Ar(16,14)=-SQR(3)*Q4r/2
2560  Ai(16,14)=-SQR(3)*Q4i/2
2570  Ar(16,15)=-Q7r/2
2580  Ai(16,15)=-Q7i/2
2590  GOSUB 2870
2600  GOSUB 3720
2610  ON Ic GOTO 2620,2640,2660,2680,2691,2693,2695,2697
2620  Freq(Ic)=D(13)-D(1)
2630  GOTO 2700
2640  Freq(Ic)=D(14)-D(2)
2650  GOTO 2700
2660  Freq(Ic)=D(15)-D(3)
2670  GOTO 2700
2680  Freq(Ic)=D(16)-D(4)
2690  GOTO 2700
2691  Freq(Ic)=D(9)-D(5)
2692  GOTO 2700
2693  Freq(Ic)=D(10)-D(6)
2694  GOTO 2700
2695  Freq(Ic)=D(11)-D(7)
2696  GOTO 2700
2697  Freq(Ic)=D(12)-D(8)
2698  GOTO 2700
2700  IF ABS(Freqq-Freq(Ic))<.05 THEN 2730
2710  Hh=Hh*(Freqq/Freq(Ic))
2720  GOTO 1240
2730  Hf(Ic)=Hh
2740  IF Ic-8=0 THEN 2770
2750  Ic=Ic+1
2760  GOTO 1230
```

```
2770  PRINT Hf(*);
2780  PRINT "/"
2790  IF K-3=0 THEN 2820
2800  K=K+1
2810  GOTO 960
2820  Beta=Beta+5
2830  IF Beta>90 THEN 2850
2840  GOTO 850
2850  CLEAR 701
2860  STOP
2870  REM ************** Subroutine 2870 ******************
2880 INTEGER U,V,W,X
2890  Tau(1,N)=1
2900  Tau(2,N)=0
2910  FOR I1=1 TO N
2920  D(I1)=Ar(I1,I1)
2930  NEXT I1
2940  FOR Ii=1 TO N
2950  U=N+1-Ii
2960  X=U-1
2970  T=0
2980  Sscale=0
2990  IF X<1 THEN 3060
3000  FOR Kcount=1 TO X
3010  Sscale=Sscale+ABS(Ar(U,Kcount))+ABS(Ai(U,Kcount))
3020  NEXT Kcount
3030  IF Sscale<>0 THEN 3090
3040  Tau(1,X)=1
3050  Tau(2,X)=0
3060  E(U)=0
3070  E2(U)=0
3080  GOTO 3660
3090  FOR K1=1 TO X
3100  Ar(U,K1)=Ar(U,K1)/Sscale
3110  Ai(U,K1)=Ai(U,K1)/Sscale
3120  T=T+Ar(U,K1)*Ar(U,K1)+Ai(U,K1)*Ai(U,K1)
3130  NEXT K1
3140  E2(U)=Sscale*Sscale*T
3150  Y=SQR(T)
3160  E(U)=Sscale*Y
3170  F=ABS(SQR(Ar(U,X)*Ar(U,X)+Ai(U,X)*Ai(U,X)))
3180  IF F=0 THEN 3270
3190  Tau(1,X)=(Ai(U,X)*Tau(2,U)-Ar(U,X)*Tau(1,U))/F
3200  Psi=(Ar(U,X)*Tau(2,U)+Ai(U,X)*Tau(1,U))/F
3210  T=T+F*Y
3220  Y=1+Y/F
3230  Ar(U,X)=Y*Ar(U,X)
3240  Ai(U,X)=Y*Ai(U,X)
3250  IF X=1 THEN 3610
3260  GOTO 3300
3270  Tau(1,X)=-Tau(1,U)
3280  Psi=Tau(2,U)
3290  Ar(U,X)=Y
3300  F=0
3310  FOR J=1 TO X
3320  Y=0
3330  Gi=0
3340  FOR K2=1 TO J
3350  Y=Y+Ar(J,K2)*Ar(U,K2)+Ai(J,K2)*Ai(U,K2)
3360  Gi=Gi-Ar(J,K2)*Ai(U,K2)+Ai(J,K2)*Ar(U,K2)
```

```
3370  NEXT K2
3380  Jp1=J+1
3390  IF X<Jp1 THEN 3440
3400  FOR K3=Jp1 TO X
3410  Y=Y+Ar(K3,J)*Ar(U,K3)-Ai(K3,J)*Ai(U,K3)
3420  Gi=Gi-Ar(K3,J)*Ai(U,K3)-Ai(K3,J)*Ar(U,K3)
3430  NEXT K3
3440  E(J)=Y/T
3450  Tau(2,J)=Gi/T
3460  F=F+E(J)*Ar(U,J)-Tau(2,J)*Ai(U,J)
3470  NEXT J
3480  Ha=F/(T+T)
3490  FOR J1=1 TO X
3500  F=Ar(U,J1)
3510  Y=E(J1)-Ha*F
3520  E(J1)=Y
3530  Fi=-Ai(U,J1)
3540  Gi=Tau(2,J1)-Ha*Fi
3550  Tau(2,J1)=-Gi
3560  FOR K4=1 TO J1
3561  O20=Fi*Tau(2,K4)+Gi*Ai(U,K4)
3570  Ar(J1,K4)=Ar(J1,K4)-F*E(K4)-Y*Ar(U,K4)+O20
3571  O21=Fi*E(K4)+Gi*Ar(U,K4)
3580  Ai(J1,K4)=Ai(J1,K4)-F*Tau(2,K4)-Y*Ai(U,K4)-O21
3590  NEXT K4
3600  NEXT J1
3610  FOR K5=1 TO X
3620  Ar(U,K5)=Sscale*Ar(U,K5)
3630  Ai(U,K5)=Sscale*Ai(U,K5)
3640  NEXT K5
3650  Tau(2,X)=-Psi
3660  Ha=D(U)
3670  D(U)=Ar(U,U)
3680  Ar(U,U)=Ha
3690  Ai(U,U)=Sscale*SQR(T)
3700  NEXT Ii
3710  RETURN
3720  REM *************** Subroutine 3720 ***************
3730  Achep=.00000001
3740  Ierr=0
3750  IF N=1 THEN 4340
3760  FOR Uu=2 TO N
3770  E(Uu-1)=E(Uu)
3780  NEXT Uu
3790  E(N)=0
3800  FOR Xx=1 TO N
3810  V=0
3820  FOR O=Xx TO N
3830  IF O=N THEN 3860
3840  IF ABS(E(O))<=Achep*(ABS(D(O))+ABS(D(O+1))) THEN 3860
3850  NEXT O
3860  Pp=D(Xx)
3870  IF O=Xx THEN 4230
3880  IF V=30 THEN 4330
3890  V=V+1
3900  Gg=(D(Xx+1)-Pp)/(2*E(Xx))
3910  Rr=SQR(Gg*Gg+1)
3920  Gg=D(O)-Pp+E(Xx)/(Gg+SGN(Gg)*Rr)
3930  S=1
3940  C=1
```

```
3950  Pp=0
3960  Mm1=0-Xx
3970  FOR Iii=1 TO Mm1
3980  Uu=0-Iii
3990  Z=S*E(Uu)
4000  Bb=C*E(Uu)
4010  IF ABS(Z)<ABS(Gg) THEN 4080
4020  C=Gg/Z
4030  Rr=SQR(C*C+1)
4040  E(Uu+1)=Z*Rr
4050  S=1/Rr
4060  C=C*S
4070  GOTO 4130
4080  S=Z/Gg
4090  Rr=SQR(S*S+1)
4100  E(Uu+1)=Gg*Rr
4110  C=1/Rr
4120  S=S*C
4130  Gg=D(Uu+1)-Pp
4140  Rr=(D(Uu)-Gg)*S+2*C*Bb
4150  Pp=S*Rr
4160  D(Uu+1)=Gg+Pp
4170  Gg=C*Rr-Bb
4180  NEXT Iii
4190  D(Xx)=D(Xx)-Pp
4200  E(Xx)=Gg
4210  E(0)=0
4220  GOTO 3820
4230  IF Xx=1 THEN 4290
4240  FOR Ii1=2 TO Xx
4250  Uu=Xx+2-Ii1
4260  IF Pp>=D(Uu-1) THEN 4300
4270  D(Uu)=D(Uu-1)
4280  NEXT Ii1
4290  Uu=1
4300  D(Uu)=Pp
4310  NEXT Xx
4320  GOTO 4340
4330  Ierr=Xx
4340  RETURN
4350  END
```

APPENDIX B

MATRIX FITTING PROGRAM

Due to the length of the matrix fitting program, I will describe it with a flowchart rather than with the program listing. The program begins by setting the values for the initial parameters and assigning constants used in the program. Then it produces and diagonalizes the Hamiltonian matrix and obtains the calculated frequencies. It then evaluates the sum of the squares of the differences between experimental and calculated frequencies for the initial parameters. It then adjusts the parameters in a systematic way and obtains a new sum. If the new sum is is smaller than the old sum, the program continues this process until it can no longer reduce the sum. At this point, it reports the final values of the parameters.

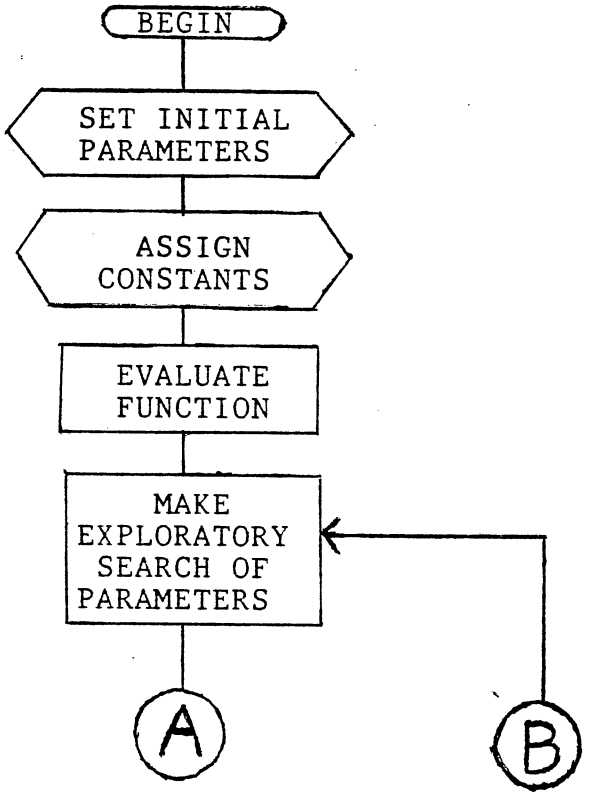

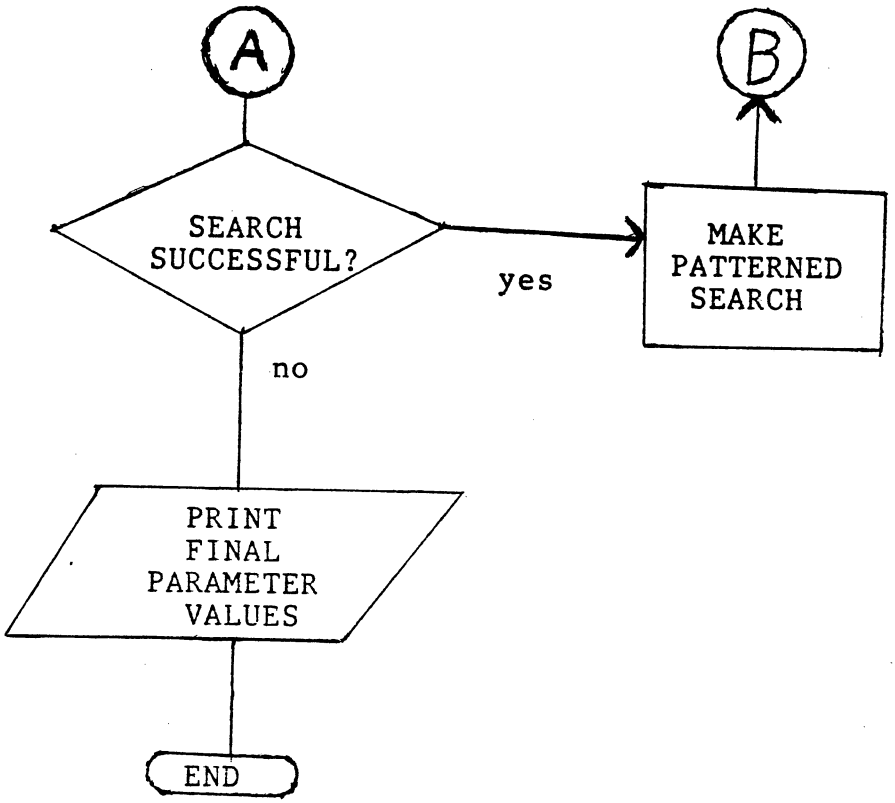
A
B
SEARCH SUCCESSFUL?
yes
MAKE PATTERNED SEARCH
no
PRINT FINAL PARAMETER VALUES
END

VITA

Mark Shannon Gulley

Candidate for the Degree of

Master of Science

Thesis: MAGNETIC RESONANCE STUDY OF RADIATION-INDUCED LITHIUM ATOMS IN CRYSTALLINE SiO_2

Major Field: Physics

Biographical:

Personal Data: Born in Fort Smith, Arkansas, May 17, 1963, the son of Roy Gene and Dora Nell Gulley.

Education: Graduated from Southside Senior High School, Fort Smith, Arkansas, in 1981, received Bachelor of Arts Degree in 1985 from Hendrix College, Conway, Arkansas; completed the requirements for the Degree of Master of Science at Oklahoma State University, Stillwater, Oklahoma, in December, 1987.